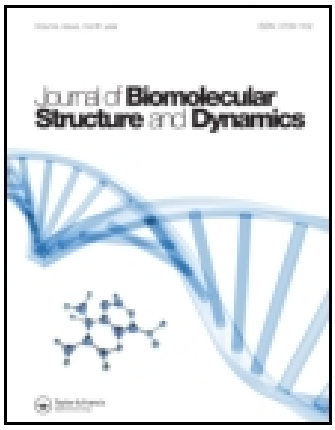

Journal of Biomolecular Structure and Dynamics
Publication details, including instructions for authors and subscription information:
http://www.tandfonline.com/loi/tbsd20

Molecular Dynamics Simulations Indicate that F87W,T185F-Cytochrome P450cam May Reductively Dehalogenate 1,1,1-Trichloroethane

John I. Manchester [a] & Rick L. Ornstein [a]
[a] Environmental Molecular Sciences Laboratory Pacific Northwest National Laboratory , Richland , WA , 99352
Published online: 21 May 2012.

To cite this article: John I. Manchester & Rick L. Ornstein (1995) Molecular Dynamics Simulations Indicate that F87W,T185F-Cytochrome P450cam May Reductively Dehalogenate 1,1,1-Trichloroethane, Journal of Biomolecular Structure and Dynamics, 13:3, 413-422, DOI: 10.1080/07391102.1995.10508851

To link to this article: http://dx.doi.org/10.1080/07391102.1995.10508851

Journal of Biomolecular Structure & Dynamics, ISSN 0739-1102
Volume 13, Issue Number 3 (1995),

Molecular Dynamics Simulations Indicate that F87W,T185F-Cytochrome P450cam May Reductively Dehalogenate 1,1,1-Trichloroethane

John I. Manchester and Rick L. Ornstein*
Environmental Molecular Sciences Laboratory
Pacific Northwest National Laboratory
Richland, WA 99352

Abstract

Cytochrome P450cam is capable of reductively dehalogenating several chlorinated alkanes at low, but measurable, rates. In previous investigations of structure-function relationships in this enzyme using molecular dynamics simulations, we noticed that 1,1,1-trichloroethane (TCA) exhibits a very high degree of mobility in the active site due to its smaller molecular volume relative to the native substrate, camphor(1,2). Several amino acid sidechains lining the active site also exhibit significant dynamic fluctuations, possibly as a result of poor steric complementarity to TCA. Guided by these results, we modeled double (F87W, T185F) and triple (F87W, T185F, V295I) mutants of P450cam, which provide additional bulk in the active site and increase the frequency of heme-substrate collision. Molecular dynamics simulations (300 ps on each protein) indicate that these mutants do not significantly perturb the three-dimensional fold of the enzyme, or local structure in the region of the active site. Both mutants bind the substrate more stably near the heme than the wild-type. Interestingly, however, the bulkier triple mutant seems to actually inhibit heme-substrate interactions relative to the double mutant. Over the final 200 ps of simulation, TCA is within 1 Å of nonbonded contact with the heme 25% more often in the double mutant *versus* the wild-type. The triple mutant, on the other hand, binds TCA within 1 Å of the heme only 15% as often as the wild-type. These results indicate that the double mutant may reductively dehalogenate TCA, a property not observed for the native protein. Implications for other experimentally measurable parameters are discussed.

Introduction

1,1,1-trichloroethane (TCA) is one of the most frequently found contaminants in groundwater (3) and in waste plumes at government (4) and industrial sites. Its wide popularity stems from excellent solvent properties: high volatility, a large dipole moment (1.78 debye), low chemical reactivity and low toxicity compared to other halogenated organic solvents. However, recent concerns regarding the health effects of TCA have been raised because it interacts with cytochromes P450 in the mammalian liver, resulting in the production of other, sometimes more toxic, chlorinated compounds (5) and hydrogen peroxide (6). Under anaerobic conditions, which may exist in poorly perfused liver tissue, reductive dehalogenation by these systems predominates (7). Because the oxygen tension in subsurface waste plumes

*Author to whom correspondence should be addressed. Phone: (509)-375-2132; Fax: (509)-375-6904; E-mail: rl_ornstein@pnl.gov

is also low, the opportunity exists for the use of P450s in remediating the heavily halogenated fraction with greater efficacy than other currently available methods. A major thrust of research in our laboratory centers on the rational redesign of cytochrome P450cam as part of a bioremediation system for faster removal of chlorinated solvents from the environment (8,9).

Cytochrome P450cam (camphor monooxygenase from the soil bacterium *Pseudomonas putida* G786 (10)) is the best characterized and most thoroughly studied P450 isozyme (11). Active research, directed at characterizing the reductive chemistry of P450cam, has revealed that it catalyzes elimination of chloride from several heavily halogenated methanes and ethanes (12-14). However, P450cam does not dehalogenate TCA at a measurable rate (12). Molecular dynamics (MD) simulations on P450cam have shown that TCA is highly mobile in the enzyme's active site, indicating that its residence time near the heme Fe may be quite low (1,2). Thus, the simulations appear to correlate well with the experimental findings. In this report we investigate the properties of TCA bound to two variants of P450cam with double (F87W, T185F) and triple (F87W, T185F, V295I) amino acid substitutions in the active site using 300 ps MD simulations. These mutants were designed to add steric bulk to regions of the active site left void when the native substrate, camphor, is replaced with the much smaller TCA molecule. Comparison with the wild-type trajectory indicates that TCA interacts more frequently with the heme Fe in the double mutant, whereas the triple mutant actually inhibits contact between the heme-Fe and TCA. This effect is not apparent until far into the simulation, emphasizing the necessity of long trajectories to model gradual rearrangements that can occur in the enzyme.

Methods

Camphor-bound cytochrome P450cam coordinates (16→15), obtained from the Brookhaven Protein Data Bank (17→16) (designation 2cpp), were used to construct the models for simulation. Hydrogens were added using Insight II (Biosym Technologies) and were oriented to maximize intramolecular hydrogen bonding with NETWORK (18→17). Titratable amino acids (Asp, Glu, Arg and Lys) and the N- and C-termini carried full charges; His 270 was doubly protonated (18→17). Mutants were constructed by substituting the sidechains of target residues with the sidechain of the appropriate amino acid in the crystallographic conformation. The non-native sidechains modeled in this way protrude into the active site and occupy space left void when the native substrate is replaced with the much smaller TCA. All 204 crystallographically resolved water molecules and an additional 3.0 Å layer of 682 waters were included in the calculation. Crystal water 515 was modeled as a sodium ion (15,18), otherwise explicit counterions were excluded. TCA was docked in the active site by assigning its carbons to the coordinates occupied by C5 and C6 of camphor in the crystal structure, with the fully substituted carbon nearest the heme-Fe.

Previous MD simulations in this laboratory employing a 3.0 Å water shell, with full charges on titratable protein residues, yielded results that correlate well with experimental data and led to experimentally confirmed predictions of the behavior of camphor analogues in the P450cam active site (19-22). While inclusion of several solvent layers would constitute a more physically accurate solvation model of the protein, this past work indicates that the dynamics of the substrate, which is sequestered from solvent in the deeply-buried P450cam active site, are relatively insensitive to the solvation model employed. Similarly, including counterions in the present simulations would greatly increase the amount of cpu time required to equilibrate the solvent before data collection for the protein could begin, and it has been indicated that their use may lead to unreliable results (23). The use of a non-bonded cutoff may provide adequate long-range electrostatic screening.

Atom-centered partial charges for the heme cofactor were assigned based on *ab*

initio potential-derived charges, and are described in detail elsewhere (24). Briefly, the heme was modeled as a ferric, pentacoordinate, high-spin Fe-porphine. Gaussian 92 (25) was used to calculate a UHF wavefunction at the 6-31g* level of theory. Atoms ligated to Fe were augmented with diffuse functions, and an all-electron, double-ζ quality basis was used on Fe (26). The CHELPG algorithm (27) was used to fit charges to the electrostatic potential due to the wavefunction, and was constrained to reproduce the calculated gas-phase dipole moment. Parameters for the harmonic and van der Waals contributions of heme to the forcefield have been described previously (19). Partial charges used for TCA reproduce its dipole moment, and have also been described elsewhere (1).

Prior to molecular dynamics, hydrogen atoms were minimized for 100 steps of steepest descents and 500 steps of conjugate gradients. Solvent molecules were then subjected to 500 steps of conjugate gradients minimization, 10,000 time-steps of dynamics, and another 500 steps of conjugate gradients minimization. The simulation protocol for the wild-type enzyme has been described previously (2) and is identical to that employed here with the exception that 5000 steps of dynamics, including protein hydrogens, were performed in the previous relaxation phase. Waters were assigned random velocities from a Maxwell-Boltzmann distribution at 50 K for 500 steps, warmed to 150 K for 4500 steps, and to 300 K for the final 5000 steps. The entire system was finally treated with 1000 steps of conjugate gradients minimization.

Molecular dynamics on the entire system commenced with the assignment of random velocities at 50 K; the system was gradually warmed to 300 K over 10,000 time-steps. Production dynamics continued for a total of 300 ps, with the system coupled to a thermal bath at 300 K (τ_T = 0.1 ps) (28). A 1.0 fs timestep was used throughout. Nonbonded interactions were evaluated using twin cutoffs of 12.0 and 15.0 Å, with interactions in the outer cutoff region updated every 20 timesteps. All molecular mechanics calculations were performed with a constant dielectric of 1.0, using the consistent-valence forcefield (cvff) (29) and Discover 2.95 (Biosym Technologies). At the cutoffs, nonbonded interactions were truncated without the fifth-order polynomial switching function implemented by Biosym, as its use has been shown to introduce artifacts (30,31). This combination of cutoffs and constant dielectric has been shown to yield reasonable results, while making efficient use of CPU time in conjunction with Discover and the cvff (31). Structures were sampled at 0.5 ps intervals for analysis. Active site volumes reported were calculated from active site molecular surfaces generated with GRASP (32), using a probe radius of 1.4 Å and Biosym radii for the protein.

Results and Discussion

To a hydrophobic substrate, the P450cam active site offers refuge from the aqueous environment of bulk solvent. Camphor binds snugly near the heme in this pocket, and under normal conditions a single product (C5-*exo*-hydroxy camphor) is formed with complete coupling of reducing equivalents (33). But for TCA and other small organics, the internal surface of this relatively large active site offers numerous, equivalently suboptimal, hydrophobic contacts to the substrate—not all of which are in proximity to the heme. Although the precise distance-dependence of electron transfer from the heme to TCA has not been determined, the probability may fall off quite rapidly with distance, so that these donor and acceptor groups must be nearly in nonbonded contact for electron transfer to occur (see, for example, ref. (34)). Therefore, poor complementarity between active site and substrate manifests itself not only in a large substrate dissociation constant (12); it contributes to the inability of the wild-type enzyme to dehalogenate TCA. It follows that mutants with active sites nestling TCA close to the heme are required if electron transfer, and subsequent elimination of chloride, are to occur.

Details of the 300 ps MD simulation on TCA-bound wild-type P450cam are report-

ed elsewhere (2), but several results are included here for comparison with the mutants. Figure 1 shows molecular surfaces of the P450cam active site after minimization and for the time-averaged atom positions over the final 200 ps of simulation. Compared to camphor, TCA exhibits poor steric complementarity to the

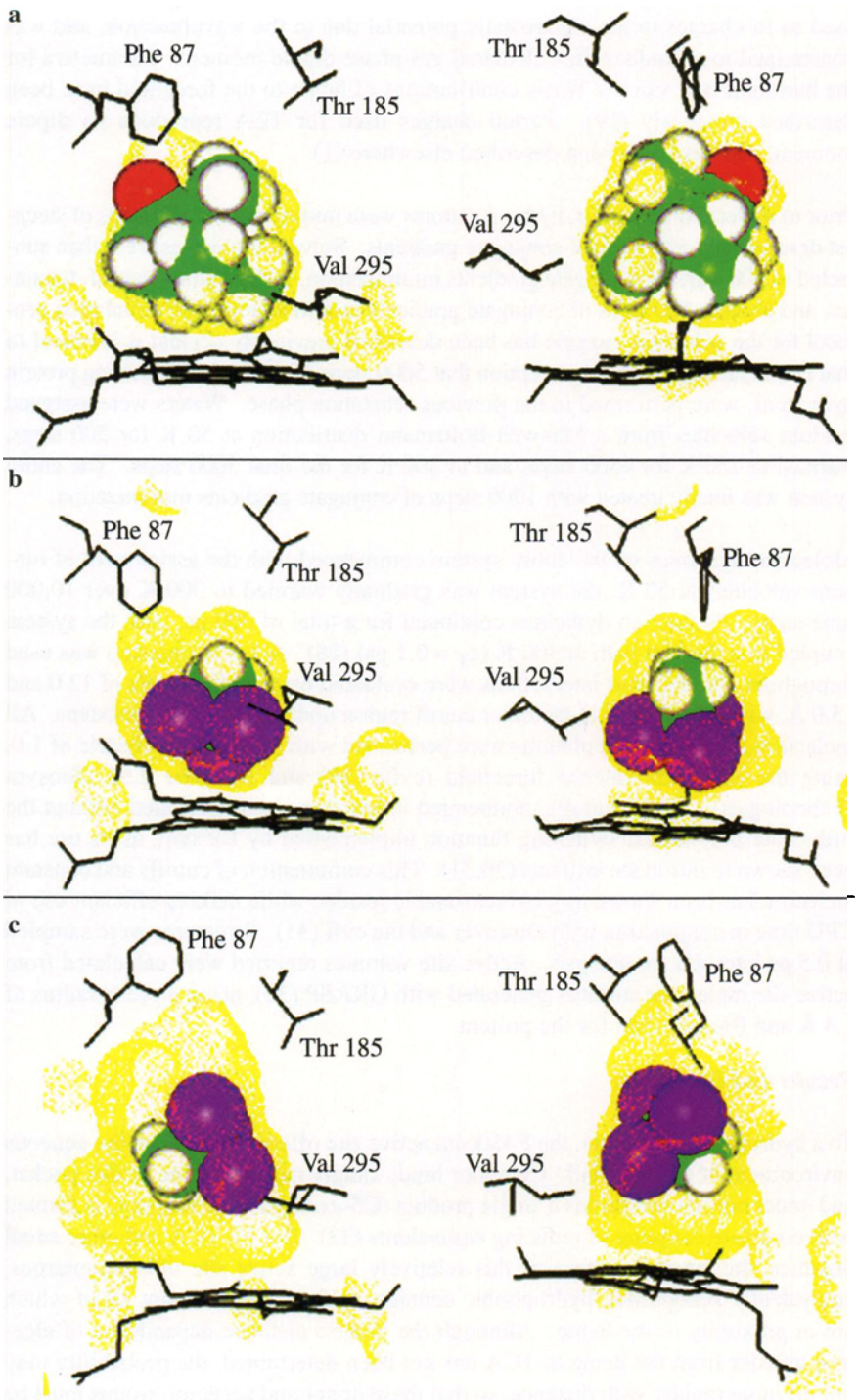

Figure 1: Molecular surfaces (gray dots) of the energy-minimized *(a,b)* wild-type P450cam active site illustrates its high degree of complementarity to the native substrate, camphor *(a)* (taken from ref. (1)). Fewer nonbond contacts are satisfied by the small TCA molecule *(b)* in this pocket. During the final 200 ps of simulation (represented by the time-averaged coordinates *(c)*), the active site expands, resulting in even less steric complementarity (2). The view on the right has been rotated by approximately 90°.

binding pocket. This condition worsens as the trajectory proceeds, evident from the time-averaged structure, primarily due to rearrangement in the sidechain of Phe 87. Flexibility in active site residues, particularly in Phe 87 since it lies in the putative substrate access channel (15), may play a cooperative role in substrate binding. However, these fluctuations are diminished in the presence of camphor (1,21,22,35,36). Greater mobility of active site residues may be a consequence of the fact that smaller molecules, such as TCA, cannot simultaneously satisfy as many stabilizing, nonbonded interactions in the wild-type active site as camphor.

Clearly, additional bulk in the region of Phe 87 is one requirement of an active site that confers a preference for TCA binding near the heme. We therefore chose to substitute Phe 87 with Trp, and Thr 185 with Phe in a double mutant. Mutations at these positions are not expected to interfere appreciably with TCA binding because it is much smaller than the native substrate. In an attempt to further increase hydrophobic contacts available to the substrate when bound near the heme, we also examined a triple mutant in which Val 295 is replaced with Ile.

	Initial[a]	Final[b]	Mean (σ)[c]
Rms Deviation from Crystal (Å)			
All Heavy Atoms	0.60	2.31	2.14 (0.16)
	0.61	2.46	1.99 (0.15)
	0.58	2.45	2.27 (0.08)
All Backbone Atoms	0.52	1.92	1.81 (0.14)
	0.54	2.12	1.64 (0.14)
	0.51	2.09	1.92 (0.08)
Backbone Atoms in Helices	0.46	1.45	1.51 (0.09)
	0.47	1.52	1.24 (0.09)
	0.45	1.74	1.61 (0.08)
Active Site Heavy Atoms[d]	0.50	1.59	1.53 (0.10)
	0.50	1.63	1.50 (0.12)
	0.55	1.53	1.50 (0.08)
Intramolecular Hydrogen Bonds[e]			
Backbone (total)	194	156	144 (7)
	190	151	146 (7)
	204	144	144 (7)
Sidechain (total)	153	120	121 (7)
	152	129	127 (7)
	148	131	123 (7)
Backbone (conserved)[f]	180	113	111 (6)
	174	107	113 (7)
	189	117	112 (5)
Sidechain (conserved)	103	31	38 (5)
	103	36	42 (6)
	105	46	45 (4)
Radius of Gyration (Å)	21.36	21.66	21.62 (0.06)
	21.38	21.70	21.68 (0.06)
	21.37	21.73	21.74 (0.05)
Rms Fluctuation in ϕ (°)	—	—	13.6 (5.6)
	—	—	13.7 (6.3)
	—	—	13.6 (7.0)
Rms Fluctuation in ψ (°)	—	—	13.8 (6.6)
	—	—	13.9 (8.2)
	—	—	13.6 (8.3)
Active Site Volume (Å^3)	206.2	484.9	451.6
	195.6	239.2	256.2
	153.8	299.2	282.6

Table I
Global dynamics properties of the wild-type (upper number), double- (middle) and triple- (lower) mutant enzymes.
[a] Energy-minimized structure, starting from crystallographic coordinates. [b] Last structure sampled. [c] Over the final 200 ps of simulation. [d] Residues within 5.0 Å of camphor in the crystal structure. [e] The number of backbone-backbone hydrogen bonds in the crystal conformation is 213; there are 125 hydrogen bonds involving sidechains. [f] That is, hydrogen bonds also present in the crystal structure.

As a gauge of the overall stability of the mutant enzymes, we monitored several global properties of the simulations. These parameters are summarized in Table I. The root-mean-square deviation (rmsd) of all heavy atoms from the crystallographic coordinates rises to approximately 1.5 Å during thermalization (first 10 ps) in each trajectory and essentially levels off between 2.0 and 2.5 Å during the final 200 ps of simulation. Minimization alone results in an rmsd of about 0.6 Å for all three enzymes. Deviation from the crystal structure is approximately 0.4 Å smaller when only backbone atoms are considered, and about 0.6 Å smaller when this analysis is confined to α-helices. The rmsd for residues that contact camphor in the crystal structure rises to an average value of 1.5 Å in all three trajectories, indicat-

ing that the active site is flexible, but that its behavior is similar in both mutants and the wild-type enzyme. Intramolecular hydrogen bonding patterns are also similar in all three simulations: the number of conserved hydrogen bonds (that is, those also present in the starting structure) involving the backbone drops by 35% to 40% of its initial value for each enzyme. A major contribution to this decrease arises from rearrangement of the hydrogen bonding pattern within the proteins: the total number of intramolecular hydrogen bonds (for both backbone and sidechains) drops by less than 25% in each enzyme. The remaining decrease in conserved hydrogen bonds is attributable to interaction with water as the proteins relax into a solvent environment. Finally, the radius of gyration increases by roughly 3%, and the rmsd in backbone torsion angles is approximately 14°. Trends in these global dynamic properties are consistent with those observed in previous MD simulations on P450cam from this laboratory (1,19).

Overall, the patterns of flexibility in the enzymes are nearly identical, confined to surface loops and turns between secondary structural elements. In both mutants, the F-G loop is more mobile than it is in the wild-type enzyme. Flexibility in this region may be enhanced by the addition of the indole N of Trp 87 as a hydrogen bond donor. For example, the carbonyl group of Met 184 interacts intermittently with Trp 87 in both mutants, whereas in the wild-type it participates mainly in hydrogen bonds with water. The integrity of the F and G helices, however, remains intact, as do the B' and I helices, although the kink in the I helix is somewhat more pronounced in the triple mutant. In both mutants Trp 87 undergoes a rearrangement, similar to Phe 87 in the wild-type, during the equilibration phase of dynamics. Even in the alternate conformation, however, the bulkier Trp sidechain is effec-

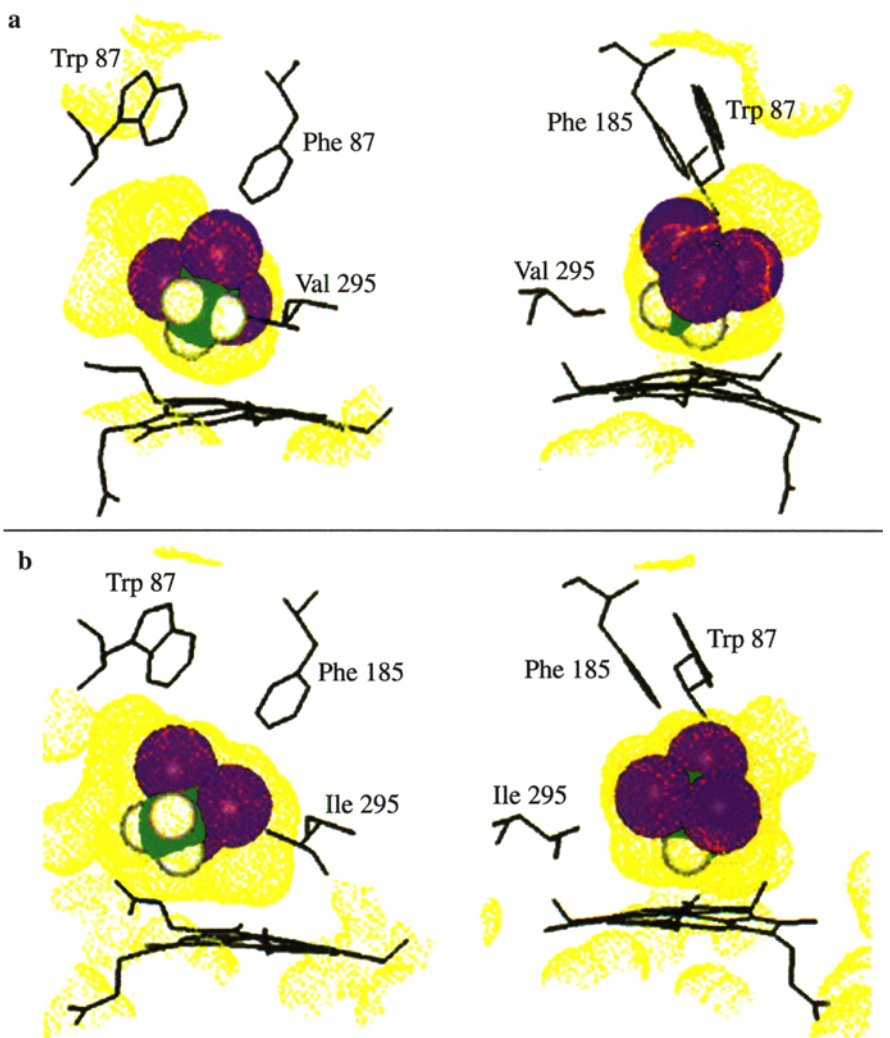

Figure 2: Molecular surfaces for time-averaged coordinates from the double (F87W, T185F) *(a)* and triple (F87W, T185F, V295I) *(b)* mutant trajectories show that much void space in the active site is filled, and steric complementarity to the substrate is improved in both P450cam variants. The volume of the time-averaged active site (see Methods) in the double mutant is only 57% of its value in the wild-type; for the triple mutant this value is, unexpectedly, slightly larger (63% of the wild-type value). The active site expands as a result of flexibility in helix I in the triple mutant. As in Figure 1, views are approximately orthogonal.

tive in reducing the size of the substrate binding pocket (Fig. 2). Fluctuations of Phe 185 are much smaller, and it remains in its initial conformation in both mutants. Ile 295 in the triple mutant also remains close to its initial conformation, although its "extra" methyl group, relative to Val, visits alternate configurations as torsion angle χ_2, samples both *gauche (+/-)* and *trans* conformations.

The volume of the wild-type active site (Table I) nearly doubles over the course of the trajectory, primarily due to the rearrangement of Phe 87 (2). The furthest extent of this pocket, in the vicinity of Phe 87, is large enough for TCA to explore. Indeed, between 175 and 250 ps (Fig. 3(a)) TCA resides in this region. That TCA returns to interact with the heme near the end of the simulation is a graphic illustration of the high degree of mobility permitted for small molecules in the wild-type binding pocket. In the double mutant, however, much of the active site void volume has been eliminated so that TCA remains in proximity to Fe during the entire simulation, and within 1 Å of Fe about 25% more often than in the wild-type trajectory. Quite the opposite is true of the triple mutant: the number of configurations sampled with TCA within 1 Å of Fe drops to only 15% of that in the wild-type. This intriguing result is a consequence of flexibility in the center of helix I: interaction with Ile 295 pushes the substrate towards Val 247 and Thr 252 on the opposite site of the active site. But flexibility in this region is not apparent from minimization alone—in fact, helix I exhibits an rmsd from the crystal structure of approximately 1.0 Å during the first 100 ps of simulation. Rather, it is a gradual rearrangement in the kink in helix I, partially accommodated by the C-terminal end of helix J, that results in this additional substrate binding surface. Although flexibility in these regions of the native protein has been observed in simulations from this (19,22) and other (37) laboratories, substitution for a bulkier amino acid at position 295 appears to exploit this pliability in the presence of substrate. The result is that the active site, during the final 200 ps of simulation, is actually about 10% larger in the triple mutant than it is in the double mutant.

The primary deviation among these simulations arises in the dynamic behavior of TCA within the active site of P450cam. Greater configurational freedom of camphor analogues in this active site has been implicated to explain deviations from the native system in experimentally observable parameters (discussed in more detail below) such as K_D, spin conversion of the heme Fe, and coupling of NADH to product formation; these factors are known to influence the catalytic efficiency of the oxidative system (11,21,22,38,39). For reductive dehalogenation, however, it appears that the rate-determining step is the first electron transfer event between the heme to the substrate, so that K_D and spin conversion do not have such a pronounced effect on the rate of reductive dehalogenation. This hypothesis is supported by the observation that calculated vertical electron affinities (VEA) for the halomethanes, which can be taken as estimates of their one-electron reduction potentials, correlate well with the rates of reductive dehalogenation observed for these molecules in the presence of P450 (40,41). We recently conducted similar calculations for the chloroethanes (manuscript in preparation) and found that the correlation holds for compounds in this class, as well. Therefore, monitoring the frequency of heme-substrate interaction in a simulation should provide information about the formation of a precursor complex between these donor and acceptor groups *in vitro* or *in vivo*, within which substrate reduction most likely occurs.

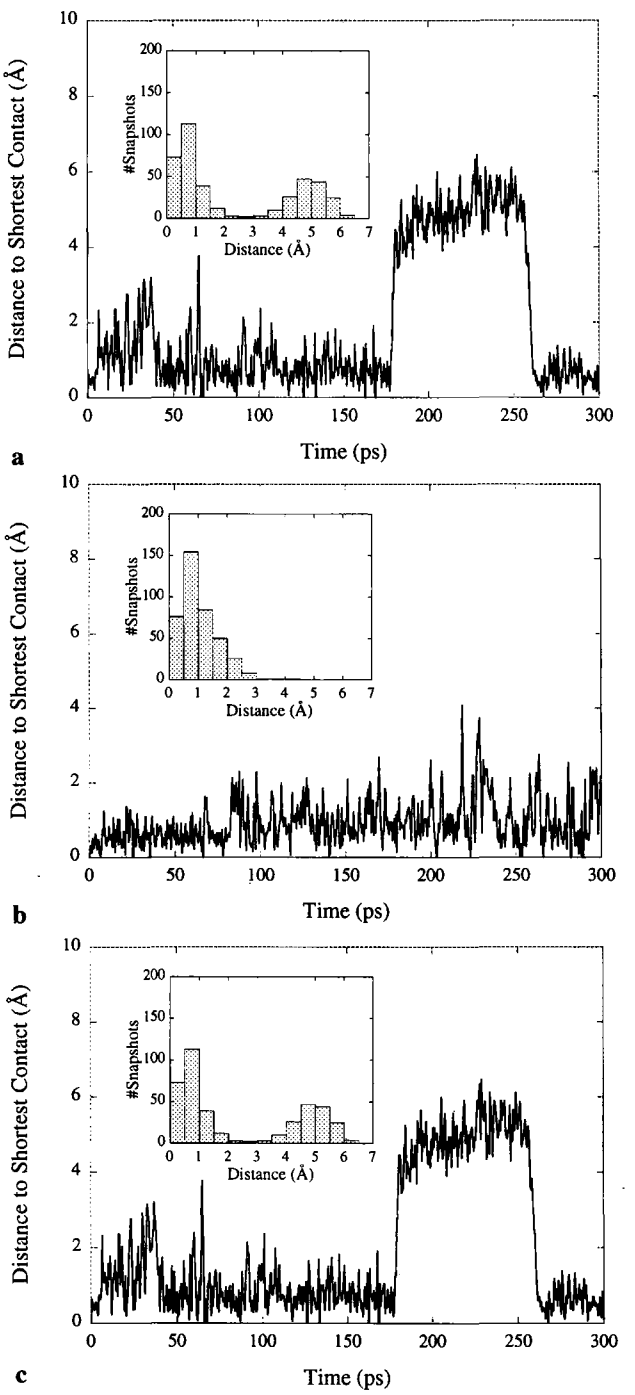

Figure 3: Heme-substrate distances, adjusted for van der Waals radii, indicate substrate mobility and have implications for the probability of electron transfer from the heme to TCA. The wild-type active site *(a)* permits a high degree of mobility, whereas both the double *(b)* and triple *(c)* mutants improve binding near the heme. The slow rearrangement in the region of helix I, however, allows TCA to bind farther than 1 Å from the heme over the final 200 ps of simulation in the triple mutant.

Figure 3 shows the distance between the heme-Fe and the closest substrate atom for each simulation. These distances have been corrected for the van der Waals radii of the respective atoms; a distance of 0.0 Å means the substrate is in contact with the heme-Fe. The insets in Fig. 3 show the distribution of Fe-substrate distances sampled over the final 200 ps (at 0.5 ps intervals). *Ab initio* molecular orbital studies on chlorinated alkanes suggest that the these compounds possess delocalized, highly diffuse LUMOs (42). Therefore, in this analysis we disregard substrate orientation and focus on the distance between the heme-Fe and any substrate atom in interpreting differences in substrate dynamics, and the expected affects on the rate of dehalogenation. The rates of dehalogenation for several chlorinated hydrocarbons have been experimentally measured, but TCA is one of several chloroethanes which falls below the detection limit in these determinations (14). According to the VEA calculations, TCA has the most favorable reduction potential of the "non-reactive" chloroethanes, indicating that only minor perturbations to factors controlling electron transfer may result in a measurable dehalogenation rate. The modest increase in Fe-TCA close contacts observed for the double mutant in the present study indicates that it may push the rate into the experimentally detectable range.

Improved substrate-active site complementarity, and more frequent heme-TCA interactions, may influence experimentally measurable quantities other than dehalogenation rate. In the resting state, P450cam has several water molecules in the active site, one of which is axially ligated to the heme-Fe (43). In this environment Fe exists in the low-spin (S=1/2) state (39). When substrate binds in this pocket, it sterically expels water, resulting in conversion of the heme-Fe to the high-spin (S=5/2) state. At saturating substrate conditions, maximal spin conversion is measured as the fraction of high spin (%HS) heme present. Camphor causes effectively 100% spin conversion, while TCA causes only 30% to 50% (12,44), indicating that complementarity between active site and substrate is necessary for efficient spin conversion. Indeed, in the crystal structure of camphor-bound P450cam, no water is crystallographically resolved between the heme and the substrate, nor is there room for water (15). Because both mutants proposed here appear to bind the substrate closer to the heme, we can infer that a larger %HS will be observed in the presence of TCA, and that the substrate dissociation constant (K_D), measured as substrate concentration at half-maximal %HS, will decrease.

Based on results from the triple mutant, we expect that it will be less effective than the double mutant at binding substrate near the heme, in causing spin conversion, and at dehalogenating TCA. That flexibility in the triple mutant, leading to a broader distribution of Fe-TCA distances, becomes apparent only after more than 100 ps of simulation indicates that longer simulations may be required for bulky substitutions in the vicinity of this flexible part of the active site. We are currently evaluating additional mutant enzymes, designed to confer enhanced substrate binding and electrostatic stabilization of developing anionic character during substrate reduction, using longer trajectories.

Acknowledgments

We express gratitude to Prof. Larry Wackett, Prof. Steve Sligar, Dr. Mark Paulsen and Dr. Ernie Mueller for stimulating discussions, and to Cary Counts for useful feedback in preparing the manuscript. Pacific Northwest Laboratory is a multiprogram national laboratory, operated for the U.S. Department of Energy by Battelle Memorial Institute under Contract DE-AC06-76RLO 1830. John Manchester has a graduate student fellowship (in the Dept. of Biophysics, Roswell Park Division, State University of New York at Buffalo) administered by Associated Western Universities. This work was supported by a grant (KP0402) from the Health Effects and Life Sciences Research Division within the Office of Health and Environmental Research of the Office of Energy Research of the U.S. Department

of Energy (RLO). Computer resources were provided in part by the National Energy Research Supercomputer Center (Livermore, CA) of the U.S. Department of Energy.

References and Footnotes

1. Paulsen, M. D.; Ornstein, R. L., *J. Comput.-Aided Mol. Design 8*, 389-404 (1994).
2. Manchester, J. I.; Paulsen, M. D.; Rein, R.; Ornstein, R. L., *Chem. Phys.* in press.
3. Westrick, J. J.; Mello, J. W.; Thomas, R. F., *J. Am. Water Works Assoc. 76*, 52 (1984).
4. Riley, R. G.; Zachara, J. M.; Wobber, F. J. "Chemical Contaminants on DOE Lands and Selection of Contaminant Mixtures for Subsurface Science Research," Report No. DE92-014826, U.S. Department of Energy (1992).
5. Casciola, L. A. F.; Ivanetich, K. M., *Carcinogenesis 5*, 543-548 (1984).
6. Takano, T.; Miyazaki, Y.; Araki, R., *Xenobiotica 18*, 1457-1464 (1988).
7. Wolf, C. R.; Harrelson, W. G.; Nastainczyk, W. M.; Philpot, R. M.; Kalyanaraman, B.; Mason, R. M., *Mol. Pharmacol. 18*, 553-558 (1980).
8. Ornstein, R. L. In *On-Site Bioreclamation: Processes for Xenobiotic and Hydrocarbon Treatment*; R. E. Hinchee and R. F. Olfenbuttel, Ed.; Butterworth-Heinemann, Stoneham MA: Columbus, OH, pp 509-514 (1991).
9. Ornstein, R. L. In *Structural Biology: State of the Art 1993*; S. R. H. and S. M. H., Ed.; Adenine Press: Albany, NY, Vol. 1; pp 59-76 (1994).
10. Hedegaard, J.; Gunsalus, I. C., *J. Biol. Chem. 240*, 4038 (1965).
11. Mueller, E.J., P.J. Loida, and S.G. Sligar, "Twenty-five Years of P450cam Research: Mechanistic Insights into Oxygenase Catalysis" in *Cytochrome P450cam*, P.R. Ortiz de Montellano, Ed., Plenum press, New York, in press (1995).
12. Li, S.; Wackett, L. P., *Biochemistry 32*, 9355-9361 (1993).
13. Logan, M. S. P.; Newman, L. M.; Schanke, C. A.; Wackett, L. P., *Biodegradation 4*, 39 (1993).
14. Loida, P. J. Ph.D. Thesis, University of Illinois at Urbana-Champaign, 1994.
15. Poulos, T. L.; Finzel, B. C.; Howard, A. J., *J. Mol. Biol. 195*, 687-700 (1987).
16. Bernstein, F. C.; Koetzle, T. F.; Williams, G. J. B.; Meyer, E. F. J.; Brice, M. D.; Rodgers, J. R.; Kennard, O.; Shimanouchi, T.; Tasumi, M., *J. Mol. Biol. 112*, 535-542 (1977).
17. Bass, M. B.; Hopkins, D. F.; Jaquysh, W. A. N.; Ornstein, R. L., *Proteins: Struct. Funct. Genetics 12*, 266-277 (1992).
18. DiPrimo, C.; Hua, G. H. B.; Douzou, P.; Sligar, S. G., *Eur. J. Biochem. 193*, 383 (1990).
19. Paulsen, M. D.; Ornstein, R. L., *Proteins: Struct. Funct. Genet. 11*, 184-204 (1991).
20. Loida, P. J.; Sligar, S. G.; Paulsen, M. D.; Arnold, G. E.; Ornstein, R. L., *J. Biol. Chem. 270*, 5326-533 (1995).
21. Paulsen, M. D.; Filipovic, D.; Sligar, S. G.; Ornstein, R. L., *Protein Science 2*, 357-365 (1993).
22. Bass, M. B.; Paulsen, M. D.; Ornstein, R. L., *Proteins Struct. Funct. Genetics 13*, 26-37 (1992).
23. van Gunsteren, W. F.; Luque, F. J.; Timms, D.; Torda, A. E., *Annu. Rev. Biophys. Biomol. Struct. 23*, 847-63 (1994).
24. Manchester, J. I.; Paulsen, M. D.; Ornstein, R. L. In *Modeling of Biomolecular Structures and Mechanisms*; Pullman *et al.*, Ed.; Kluwer Academic Publishers: Dordrecht, Holland, pp 181-188 (1995).
25. Frisch, M. J.; Trucks, G. W.; Head-Gordon, M.; Gill, P. M. W.; Wong, M. W.; Foresman, J. B.; Johnson, B. G.; Schlegel, H. B.; Robb, M. A.; Replogle, E. S.; Gomperts, R.; Andres, J. L.; Raghavachari, K.; Binkley, J. S.; Gonzalez, C.; Martin, R. L.; Fox, D. J.; Defrees, D. J.; Baker, J.; Stewart, J. J. P.; Pople, J. A. In Gaussian, Inc.: Pittsburgh PA, (1992).
26. Wachter, A. J. H., *J. Chem. Phys 52*, 1033 (1970).
27. Breneman, C. M.; Wiberg, K. B., *J. Comp. Chem. 11*, 361-373 (1990).
28. Berendsen, H. J. C.; Postma, J. P. M.; van Gunsteren, W. F.; DiNola, A.; Haak, J. R., *J. Chem. Phys. 81*, 3684-3690 (1984).
29. Hagler, A. T. In *The Peptides*; V. J. Hruby and J. Meienhofer, Ed.; Academic Press: New York; Vol. 7; pp 213-299 (1985).
30. Lau, K. F.; Alper, H. E.; Thacher, T. S.; Stouch, T. R., *J. Phys. Chem. 98*, 8785-8792 (1994).
31. Arnold, G. E.; Ornstein, R. L., *Proteins: Struct. Funct. Genet. 18*, 19-33 (1994).
32. Nicholls, A.; Sharp, K. A.; Honig, B., *Proteins: Struct. Funct. Genet. 11*, 282

(1991).
33. Gelb, M. H.; Heimbrook, D. C.; Malkonen, P.; Sligar, S. G., *Biochemistry 21*, 370-379 (1982).
34. Bolton, J. R.; Archer, M. D. In *Electron Transfer in Inorganic, Organic and Biological Systems*; N. Mataga and G. McLendon, Ed.; American Chemical Society: Washington, D.C.; Vol. 228; pp. 7-23 (1991).
35. Paulsen, M. D.; Bass, M. B.; Ornstein, R. L., *J. Biomolec. Struct. Dynamics 9*, 187-203 (1991).
36. Paulsen, M. D.; Ornstein, R. L., *J. Comp-Aided Molec. Design 6*, 449-460 (1992).
37. Harris, D. L.; Loew, G. H., *J. Am. Chem. Soc. 116*, 11671-11674 (1994).
38. Raag, R.; Poulos, T. L., *Biochemistry 30*, 2674-2684 (1991).
39. Sligar, S. G., *Biochemistry 15*, 5399-5406 (1976).
40. Luke, B. T.; Loew, G. H.; McLean, A. D., *J. Am. Chem. Soc. 110*, 3396-3400 (1988).
41. Waller, C. L.; McKinney, J. D., *J. Comput. Chem. 14*, 1575-1579 (1993).
42. Falcetta, M. F.; Jordan, K. D., *J. Phys. Chem. 94*, 5666 (1990).
43. Poulos, T. L.; Finzel, B. C.; Howard, A. J., *Biochemistry 25*, 5314 (1986).
44. Sligar, S. G., personal communication (1994).

Date Received: June 22, 1995

Communicated by the Editor R. H. Sarma